AIMS Mathematics, 10(8): 18024–18054.
DOI: 10.3934/math.2025803
Received: 21 June 2025
Revised: 27 July 2025
Accepted: 30 July 2025
Published: 08 August 2025

https://www.aimspress.com/journal/Math

Research article

SEIR-VQ model for the NB.1.8.1 COVID-19 variant: Mathematical analysis and numerical simulations

Faiza Arif[1,‡], Sana Ullah Saqib[2,‡], Yin-Tzer Shih[2,*] and Aneela Kausar[3]

[1] Abdus Salam School of Mathematical Sciences, Government College University, Lahore 54600, Pakistan

[2] Department of Applied Mathematics, National Chung Hsing University, Taichung 40227, Taiwan

[3] Department of Computer Science and Information Engineering, National Yunlin University of Science and Technology, Yunlin 64002, Taiwan

* **Correspondence:** Email: yintzer_shih@email.nchu.edu.tw; Tel: +886422853459; Fax: +886422873028.

Abstract: This the study proposes a novel susceptible, exposed, infectious, recovered, vaccinated, and quarantined (SEIR-VQ)-type compartmental model specifically designed to capture the transmission dynamics of the NB.1.8.1 variant of COVID-19, a recently emerged virus known for its higher transmissibility and reduced vaccine effectiveness. The model divides the population into six distinct compartments: Susceptible, exposed, infectious, quarantined, recovered, and vaccinated. The proposed formulation reflects key contemporary epidemiological factors, such as waning immunity, partial vaccine effectiveness due to viral mutations, and infectivity during quarantine. Additionally, the study conducts both dimensional and non-dimensional analyses of the system, establishes the positivity and boundedness of solutions, and derives the basic reproduction number, $\mathcal{R}_0$. It also examines the local and global stability of the disease-free equilibrium with respect to $\mathcal{R}_0$. Numerical solutions utilizing the Runge-Kutta (RK4) method and MATLAB's ode45 solver are used to simulate infection dynamics. Finally, a sensitivity analysis evaluates the influence of the key parameters that most significantly impact disease spread. The findings indicate that increasing vaccine efficacy, reducing transmission through non-pharmaceutical interventions, and enhancing the isolation of infectious individuals are effective strategies for controlling the spread of the NB.1.8.1 variant. These results support public health policies by highlighting effective control strategies.

Keywords: NB.1.8.1 COVID-19; mathematical modeling; stability analysis; sensitivity analysis; virus-free equilibrium; basic reproductive number; public health policy
Mathematics Subject Classification: 26A33, 34A08, 34A34, 65L20, 92B20, 92D30

1. Introduction

COVID-19, caused by the SARS-CoV-2 virus, continues to change with time. A recent version of the virus is called NB.1.8.1, which emerged in early 2025. This variant appears to spread more rapidly than earlier forms and may be less susceptible to current vaccines. Although the World Health Organization (WHO) states that NB.1.8.1 has not yet shown signs of causing more severe illness, it is spreading more rapidly in some regions. It has already been detected in approximately 10% of cases worldwide. This makes it essential to study how the virus behaves and find ways to control its spread.

To understand how diseases spread, researchers often develop mathematical models [1]. These models divide the population into different categories like susceptible (S), exposed (E), infected (I), and recovered (R). Such models are called compartmental models. They help predict the course of an outbreak and shape health policies. Over time, many scientists have expanded these models by adding additional groups; for example, [2] includes groups for people who are vaccinated (V) or those placed in quarantine (Q).

In this paper, we propose a realistic model, referred to as the SEIR-VQ model. It includes vaccinated and quarantined groups, both of which are crucial for controlling COVID-19 today. Compared with earlier work, such as the model by Anwar et al. [3], our model captures key features, including vaccination and isolation. This makes the model easier to analyze while accurately reflecting real-life situations.

Several studies from 2019 to 2025 have focused on modeling the spread of COVID-19 variants. For example, Tchoumi et al. employed a two-strain model in a recent study to investigate outbreaks in Europe, demonstrating how changes in vaccine effectiveness can impact the results [4]. Another survey by Chatterjee et al. used network-based models to analyze how infection and vaccination spread through communities [5]. These models provide valuable insights but are often complex and difficult to solve by hand. Some models include many parameters, which makes them difficult to analyze without a computer.

There is a growing interest in using simpler yet flexible mathematical models that can still accurately represent real-world effects, such as reinfection, partial vaccination, and quarantine. In situations where exact solutions are difficult to find, numerical methods like the RK4 and MATLAB's ode45 solver are often used. These methods generate approximate solutions by solving the system with good accuracy. Although they do not provide analytical solutions, they are effective, reliable, and relatively straightforward to implement compared with some analytical approaches, especially for models that include a large number of compartments and parameters, which often cannot be solved analytically. To study one such model, Arif et al. applied RK4 and MATLAB's ode45 solver to analyze the spread of COVID-19, considering the key features like temporary immunity and a quarantined population. They performed a detailed mathematical analysis to explore how these factors influence disease transmission [6]. Recent studies in fractional-order epidemic modeling provides new tools for understanding behavioral effects during pandemics. For example, Farman et al. proposed a fractional-order model that explores how panic spreads in response to COVID-19 [7]. In another study, Choudhary et al. investigated how environmental factors, such as ammonia levels, relative humidity, and airborne particulates like $PM_{2.5}$ and PM_{10}, are linked to COVID-19 and mortality across different regions; their findings suggest that these variables significantly influence transmission and could help

[‡]These authors contributed equally to this work

develop more effective, climate-aware disease mitigation strategies [8].

As of now, limited research has been conducted on a newly identified COVID-19 variant, which emerged in 2025. To address this gap, we aim to study its transmission dynamics using a compartmental model, with numerical simulations obtained using the RK4 method and MATLAB's ode45 solver. Recent studies by Murphy et al. highlight reports on the spread of this variant from Asia to the UK and raise concerns about its increased transmissibility and public health implications [9]. Additionally, another study by Duo et al. analyzed the antigenic and virological properties of variants such as BA.3.2, XFG, and NB.1.8.1, emphasizing their immune escape potential and impact on vaccine performance [10].

Mathematical models play a crucial role in improving our understanding of infectious disease transmission and guiding effective control strategies. For chronic viral infections like human immunodeficiency (HIV) and hepatitis B, these models offer a helpful framework for evaluating how different interventions, such as treatment programs and public awareness campaigns, can reduce transmission and improve long-term health outcomes. Because disease dynamics often involve randomness due to biological variability or external factors, adding stochastic elements to the models gives a more accurate picture. For instance, a recent study on HIV/AIDS used a stochastic control approach to evaluate the combined effects of education and treatment, providing insights into how targeted interventions can be optimized amid uncertainty [11]. Similarly, research on hepatitis B has shown how delays in transmission and direct cell-to-cell spread can lead to complex and sometimes unpredictable patterns, especially when random fluctuations are considered [12]. In another study, Saqib et al. proposed a novel hybrid fractional-order model to study the nonlinear transmission dynamics of HIV among men who have sex with men in Taiwan. Their model effectively combines fractional calculus with classical epidemiological compartments to better analyze memory effects and hereditary properties intrinsic to disease progression [13]. The model is unique in its ability to represent enduring behavioral impact on transmission rates. Its sophisticated analytical framework presents a significant basis for formulating designed intervention strategies in high-risk populations. This novel approach has the potential to inform the development of more flexible and realistic public health strategies tailored to ending the epidemic. These works highlight the growing importance of utilizing mathematically robust yet flexible models to inform effective strategies for managing chronic viral infections.

In this study, we propose a mathematical model that includes several important features.

1. A vaccinated group (V), which allows for studying how well vaccination reduces infection and how immunity may fade over time.
2. A quarantine compartment (Q), representing the effect of isolating infected people in reducing the spread of disease.
3. A time-dependent infection rate $\beta(t)$, which accounts for variations in infection risk due to factors such as the emergence of new variants or changes in public health measures.
4. Mathematical analysis, including:
    - Whether all the population groups in each compartment stay positive and bounded over time;
    - whether the disease will disappear or persist in the population, using the basic reproduction number $\mathcal{R}_0$;
    - how sensitive the model is to small changes in vaccination rates, behavior, or parameters that can stop the outbreak;

5. an application of the RK4 and MATLAB's ode45 solver to find numerical solutions;
6. numerical tests to validate the results and see the impact of various parameters on disease spread.

The present study generalizes the six-compartment SVEIQR model proposed by Haq et al. [19] by introducing several realistic and novel features specifically designed to capture the transmission dynamics of the NB.1.8.1 variant. While Haq et al. [19] studied COVID-19 transmission under the assumptions of permanent immunity and ideal vaccine-induced protection, our model incorporates waning immunity, allowing for the possibility of reinfection among both recovered and vaccinated individuals. It also accounts for partial vaccine efficacy and breakthrough infections, providing a more accurate representation of the current epidemiological variants. Additionally, we introduce a time-dependent transmission rate $\beta(t)$ to reflect evolving public health conditions. On the theoretical front, this study advances mathematical analysis by establishing global stability results using Lyapunov functions and deriving a sensitivity-based expression for the basic reproduction number $\mathcal{R}_0$. These enhancements facilitate a more comprehensive understanding of how small variations in key parameters influence disease dynamics. These improvements support more responsive, data-driven simulations, aiding in the development of timely and effective control measures, such as vaccination, isolation, and booster strategies interventions.

Recent works have explored various aspects of infectious disease modeling and control. Ramponi et al. formulated an SVIR-based model to investigate how optimal strategies for vaccination and social distancing can minimize the progression of the virus [14]. Venkatesh et al. developed a fractional-order model to capture the transmission dynamics of monkeypox in vaccinated individuals, highlighting the influence of memory effects on disease spread [15]. Meanwhile, Li et al. analyzed data on 24 notifiable diseases in China, showing how the COVID-19 pandemic affected their temporal patterns and public health response [16]. Recent contributions such as the work by Peng Wu et al. explore a space- and age-structured COVID-19 model that combines within-host infection processes with between-host transmission dynamics. Their findings suggest that infection age and spatial diffusion are essential in shaping the epidemic's course and therefore must be included in realistic models [17]. These studies demonstrate that incorporating compartments for vaccinated and quarantined individuals enhances the accuracy of epidemic models. They also emphasize the need to strike a balance between model simplicity and the realistic representation of disease dynamics.

Figure 1 presents data from BBC News showing the NB.1.8.1 variant of COVID-19 cases reported on or prior to June 7, 2025.

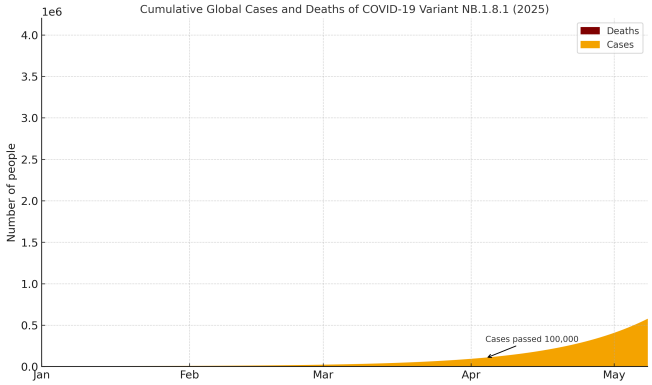

Figure 1. BBC News (accessed 7 June 2025).

The main objectives of the present study are to analyze an SEIR-VQ model tailored to the NB.1.8.1 variant, prove the positivity and boundedness of the system, calculate and interpret the basic reproduction number $\mathcal{R}_0$, analyze both the local and global stability, perform numerical simulations using the RK4 and ode45, and carry out a sensitivity analysis to identify key parameters influencing disease spread.

This model provides valuable insights for planners to better understand how to respond quickly and more effectively to rapidly spreading new COVID-19 variants. The simple structure of the proposed model also makes it easy to extend further.

To meet this objective, the paper is organized into three core sections. Section 2 outlines the formulation of the mathematical model. Section 3 focuses on the normalization, positivity, and boundedness of the system. Moreover, it discusses the stability analysis and examines the existence of equilibrium points. Section 4 presents the numerical simulations and graphical illustrations to support the theoretical findings.

2. Model formulation

The classical SIR model, first introduced by Kermack and McKendrick in the early 20$^{\text{th}}$ century, represents one of the earliest mathematical models for analyzing infectious diseases by dividing the population into susceptible, infected, and recovered groups [18]. Over time, this foundational model has been extended into more detailed structures, each capturing additional epidemiological aspects.

The present study significantly extends the SVEIQR model proposed by Haq et al. [19], emphasizing the roles of vaccination and quarantine in controlling COVID-19 transmission. Although both models include exposed, quarantined, and vaccinated groups, our SEIR-VQ model adds several new epidemiological features, making it more relevant to the dynamics of the 2025 NB.1.8.1 variant. One major enhancement is the addition of waning immunity, which allows recovered and vaccinated individuals to re-enter the susceptible class. This feature was not previously included considered.

Furthermore, our model considers vaccination as time-sensitive and only partially effective, enabling the simulation of breakthrough infections, a phenomenon increasingly observed with emerging variants. It also incorporates a time-dependent transmission rate, $\beta(t)$, which captures temporal fluctuations in transmissibility caused by viral evolution or public health measures. In contrast, the model proposed by Haq et al. [19] assumes a constant transmission rate throughout the analysis. From a mathematical perspective, the model is supported by a thorough theoretical analysis, including the positivity and boundedness of the solutions, global stability using Lyapunov functions, and normalized sensitivity analysis of the basic reproduction number $\mathcal{R}_0$. These features offer deeper insights into long-term behavior and help inform public health strategies under changing epidemiological conditions.

To understand the transmission dynamics of the NB.1.8.1 variant of COVID-19, we propose a compartmental model that divides the total population into six distinct epidemiological compartments: susceptible (S), exposed (E), infectious (I), quarantined (Q), recovered (R), and vaccinated (V). This model emphasizes the roles of waning immunity, vaccination, and quarantine. The total population at time t is given by:

$$N = S + E + I + R + V + Q.$$

Model assumptions:

The proposed model is based on these key assumptions:

- Vaccination offers partial protection, with effectiveness represented by $\eta \in [0, 1]$. Vaccinated individuals can still be infected but face a lower risk.
- Recovered individuals do not have permanent immunity; they may lose immunity at a rate ω, returning to the susceptible class.
- Infectious individuals are isolated at a rate θ, moving into the quarantined group Q, where they can still spread the disease at a reduced rate ($\xi \in [0, 1]$).
- Disease-related deaths happen in both the I and Q groups, at rates of δ and δ_q respectively.
- The infection rate $\beta(t)$ is time-dependent to reflect changing public health conditions or new variants' behavior.

Governing equations:
The following system of ordinary differential equations describes the dynamics of the disease:

$$\begin{aligned}
\frac{dS}{dt} &= -\beta(t)\,(I + \xi Q)\,\frac{S}{N} - \nu S + \omega R,\\
\frac{dE}{dt} &= \beta(t)\,(I + \xi Q)\left(\frac{S}{N} + (1-\eta)\,\frac{V}{N}\right) - \sigma E,\\
\frac{dI}{dt} &= \sigma E - (\theta + \gamma + \delta)\,I,\\
\frac{dR}{dt} &= \gamma I + \gamma_q Q - \omega R,\\
\frac{dV}{dt} &= \nu S - (1-\eta)\beta(t)\,(I + \xi Q)\,\frac{V}{N},\\
\frac{dQ}{dt} &= \theta I - (\gamma_q + \delta_q)\,Q.
\end{aligned}$$

The transmission potential in the proposed model is determined by a set of interconnected parameters designed to accurately represent the progression and spread of the disease within a population. A key component is the time-dependent transmission rate $\beta(t)$, which enables the model to account for changes in contact behavior and seasonal variations over time. The parameter η denotes vaccine efficacy, emphasizing that vaccinated individuals can still acquire and transmit infection, though at lower levels. Quarantined individuals are modeled to have reduced but nonzero infectiousness, controlled by the parameter ξ, to capture potential transmission from isolated cases caused by delayed detection or imperfect containment. The infection spreads through contact between susceptible individuals and both quarantined and actively infectious individuals. The total infectious pressure is modeled as:

$$\beta(t)(I + \xi Q),$$

where ξ captures the relative infectiousness of isolated individuals compared with non-isolated ones. Both vaccinated and susceptible individuals are exposed to infection, with vaccinated individuals experiencing reduced susceptibility due to the vaccine's efficacy.

Each equation depicts the inflow and outflow of individuals in the corresponding compartment. Table 1 outlines the definitions of the population compartments included in the model.

Table 1. Description of the population compartments.

Groups	Description
S	Individuals who are vulnerable to infection by contact with infectious or quarantined individuals, vaccinated at a rate ν, and refilled by waning immunity from the recovered class
E	Those carrying the infection in its early stage but are not yet infectious; they can progress to the infectious class
I	Individuals capable of transmitting the virus to others; they can be quarantined, can recover, or die
R	Individuals who have recovered, deceased, or have a possibility of reinfection due to waning immunity
V	Individuals who received the vaccination but remain partially at risk of infection due to reduced efficacy
Q	Individuals placed in isolation after testing positive for the virus

The model's parameters, each of which is assumed to be positive, are summarized in Table 2.

Table 2. Description of the model's parameters.

Symbol	Meaning
$\beta(t)$	Infection transmission rate (may vary over time)
ν	Vaccination rate at which susceptible individuals are vaccinated
η	Effectiveness of vaccine
ξ	Level of infectiousness of the quarantined group of people compared with infectious ones
σ	Rate at which exposed individuals become infectious
θ	Rate of isolation of infectious individuals
γ, γ_q	Recovery rates for infected and quarantined individuals, respectively
δ, δ_q	Death rates for infected and isolated individuals
ω	Rate of waning immunity from recovered to being susceptible again

3. Mathematical analysis

3.1. Non dimensionalization of the SEIR-VQ model

To simplify the analysis and reduce the number of parameters, we perform a non-dimensionalization of the proposed SEIR-VQ model for the NB.1.8.1 variant. This transformed form of the model facilitates a more efficient understanding of the model's behavior.

The step-by-step procedure is as follows:

Step 1. Define scaled variables

Begin by normalizing each compartment by the total population size N and then rescaling the time using the recovery rate γ

$$\tau = \gamma t \quad \text{(dimensionless time)},$$

Define the following normalized variables:

$$s = \frac{S}{N}, \quad v = \frac{V}{N}, \quad e = \frac{E}{N}, \quad i = \frac{I}{N}, \quad q = \frac{Q}{N}, \quad r = \frac{R}{N}.$$

The population constraint now becomes

$$s + v + e + i + q + r = 1.$$

Step 2. Introduce dimensionless parameters

Expressing all the rates relative to the reference rate γ as follows:

$$\tilde{\beta}(\tau) = \frac{\beta(t)}{\gamma}, \quad \tilde{\nu} = \frac{\nu}{\gamma}, \quad \tilde{\sigma} = \frac{\sigma}{\gamma}, \quad \tilde{\theta} = \frac{\theta}{\gamma}, \quad \tilde{\delta} = \frac{\delta}{\gamma}, \quad \tilde{\delta}_q = \frac{\delta_q}{\gamma}, \quad \tilde{\gamma}_q = \frac{\gamma_q}{\gamma}, \quad \tilde{\omega} = \frac{\omega}{\gamma}.$$

We also denote time in terms of τ as

$$\tilde{t} = \tau = \gamma t.$$

Step 3. Reformulate the system

The set of original equations now takes the following normalized form:

$$\frac{ds}{d\tau} = -\tilde{\beta}(\tau)(i + \xi q)s - \tilde{\nu}s + \tilde{\omega}r, \tag{3.1}$$

$$\frac{dv}{d\tau} = \tilde{\nu}s - (1 - \eta)\tilde{\beta}(\tau)(i + \xi q)v, \tag{3.2}$$

$$\frac{de}{d\tau} = \tilde{\beta}(\tau)(i + \xi q)\,(s + (1 - \eta)v) - \tilde{\sigma}e, \tag{3.3}$$

$$\frac{di}{d\tau} = \tilde{\sigma}e - (\tilde{\theta} + 1 + \tilde{\delta})i, \tag{3.4}$$

$$\frac{dq}{d\tau} = \tilde{\theta}i - (\tilde{\gamma}_q + \tilde{\delta}_q)q, \tag{3.5}$$

$$\frac{dr}{d\tau} = i + \tilde{\gamma}_q q - \tilde{\omega}r, \tag{3.6}$$

which satisfies the following initial state of the system:

$$s(0) = s_0,\ e(0) = e_0,\ i(0) = i_0,\ r(0) = r_0,\ v(0) = v_0,\ q(0) = q_0 \geq 0.$$

Normalizing the total population to unity as follows:

$$s_0 + v_0 + e_0 + i_0 + q_0 + r_0 = 1.$$

However, the effective change due to disease-related mortality is reflected as

$$\frac{d}{d\tau}(s + v + e + i + q + r) = -\tilde{\delta}i - \tilde{\delta}_q\, q \leq 0.$$

This indicates that the total population decreases over time due to deaths caused by the disease in both the infectious and quarantined classes.

3.2. Positivity of solutions

To ensure that the model remains biologically meaningful, we prove that all state variables stay non-negative for all times $\tau \geq 0$.

Lemma 3.1. *(Positivity and boundedness) For any non-negative initial values, we have*

$$\mathbf{y}_0 = (s(0), v(0), e(0), i(0), q(0), r(0)) \in \mathbb{R}^6_+ \quad with \quad \sum_{j=1}^{6} y_j(0) = 1,$$

the solution $\mathbf{y}(\tau)$ *to system* (3.1) *exists, remains non-negative, and is bounded for all* $\tau \geq 0$*. That is,*

$$y_j(\tau) \geq 0, \quad \forall\, \tau \geq 0, \quad j = 1, \ldots, 6,$$

and

$$\sum_{j=1}^{6} y_j(\tau) \leq 1, \quad \forall\, \tau \geq 0.$$

Proof. Each equation in the system (3.1) can be expressed as the difference between the non-negative inflow and outflow terms. To verify positivity, suppose $y_j = 0$ for some component. Since all outflow terms are proportional to y_j, they vanish at the boundary, and inflow terms (depending on other $y_k \geq 0$) remain non-negative.
Thus

$$\left.\frac{dy_j}{d\tau}\right|_{y_j=0} \geq 0.$$

This ensures that no variable becomes negative.
Now, summing all equations

$$\frac{d}{d\tau}(s + v + e + i + q + r) = -\tilde{\delta} i - \tilde{\delta}_q q \leq 0,$$

indicates a non-increasing total due to disease-related mortality.
Hence,

$$\sum_{j=1}^{6} y_j(\tau) \leq \sum_{j=1}^{6} y_j(0) = 1.$$

Each equation in the system is composed of gain and loss terms, where all expressions are either directly proportional to the state variables or involve non-negative quantities. Given that the right-hand sides of the system are Lipschitz continuous and the model is mathematically well-posed, classical results from the theory of ordinary differential equations guarantee that the solutions remain non-negative for all $\tau \geq 0$. □

3.3. Boundedness of the solutions

Next, we show that the solutions remain bounded within the biologically feasible region.

$$\Omega = \left\{(s, v, e, i, q, r) \in \mathbb{R}^6_+ \,\middle|\, s + v + e + i + q + r = 1\right\}.$$

Taking the total derivative of the sum of all compartments, we have

$$\frac{d}{d\tau}(s + v + e + i + q + r) = 0.$$

This implies that the total normalized population remains constant over time.

$$s(\tau) + v(\tau) + e(\tau) + i(\tau) + q(\tau) + r(\tau) = 1, \quad \forall \tau \geq 0.$$

Therefore, all the compartment values remain bounded within the interval [0, 1], and the system evolves within the positively invariant set Ω.

3.4. Disease-free equilibrium

Disease-free equilibrium (DFE) corresponds to the steady state where no infection exists in the population, i.e., all infected compartments are zero.

$$e = 0, \quad i = 0, \quad q = 0.$$

At this point, the remaining compartments, s, v, and r, represent the distribution of the healthy population. After some manipulations, we obtain the following DFE:

$$(s_0, v_0, e_0, i_0, q_0, r_0) = (0,\ 1,\ 0,\ 0,\ 0,\ 0).$$

This implies that there will be no infection if the entire population is vaccinated.

3.5. Basic reproductive number $\mathcal{R}_0$

To determine the basic reproduction number $\mathcal{R}_0$ for the normalized SEIR-VQ model describing the dynamics of the modern COVID-19 variant (NB.1.8.1), we employ the following generation matrix approach.

Step 1. Identification of infected compartments Only compartments e and i contribute to the generation of new infections, while q (isolation) does not directly spread the infection, though it modulates transmission via a reduced factor ξ.

Step 2. Linearization At the DFE, the Jacobian matrices of $\mathcal{F}$ and $\mathcal{V}$ with respect to the infected variables $[e, i, q]^T$ are

$$\mathcal{F} = \begin{bmatrix} 0 & \tilde{\beta}(1-\eta) & \tilde{\beta}\xi(1-\eta) \\ 0 & 0 & 0 \\ 0 & 0 & 0 \end{bmatrix},$$

$$\mathcal{V} = \begin{bmatrix} \tilde{\sigma} & 0 & 0 \\ -\tilde{\sigma} & \tilde{\theta} + 1 + \tilde{\delta} & 0 \\ 0 & -\tilde{\theta} & \tilde{\gamma}_q + \tilde{\delta}_q \end{bmatrix}.$$

Step 3. Next-generation matrix and $\mathcal{R}_0$

The next-generation matrix is defined as [20, 21]:

$$\mathcal{K} = \mathcal{F}\mathcal{V}^{-1}.$$

After computing $K = FV^{-1}$, we obtain the basic reproduction number

$$\mathcal{R}_0 = \tilde{\beta}(1-\eta)\Big(\frac{\tilde{\gamma}_q + \tilde{\delta}_q + \xi\tilde{\theta}}{(\tilde{\theta} + 1 + \tilde{\delta})(\tilde{\gamma}_q + \tilde{\delta}_q)}\Big).$$

It can be interpreted as follows:

- $\mathcal{R}_0$ increases with an increase in the transmission rate $\tilde{\beta}$, a decrease in vaccine efficacy η, and greater relative infectiousness of individuals under quarantine ξ.
- Higher vaccine efficacy η and rapid isolation $\tilde{\theta}$ contribute to reducing $\mathcal{R}_0$.
- Higher recovery $\tilde{\gamma}_q$ or mortality rates $\tilde{\delta}_q$ in quarantine accelerate the removal of infectiousness, thereby decreasing $\mathcal{R}_0$.
- An increase in the combined removal rate of infected individuals $(\tilde{\theta}+1+\tilde{\delta})$ in the non quarantined group helps curb transmission, thereby reducing $\mathcal{R}_0$.

3.6. Local stability

The following theorem states the local stability behavior of the system around the DFE:

Theorem 3.2. *The DFE of the system is locally asymptotically stable if and only if the basic reproduction number is $\mathcal{R}_0 < 1$. Conversely, if $\mathcal{R}_0 > 1$, then the DFE is unstable.*

To analyze the local behavior of the system near the DFE, linearization of the model around the DFE results in the following Jacobian matrix J of the infected subsystem:

$$J = \begin{bmatrix} -\tilde{\sigma} & \tilde{\beta}(1-\eta) & \tilde{\beta}\xi(1-\eta) \\ \tilde{\sigma} & -(\tilde{\theta}+1+\tilde{\delta}) & 0 \\ 0 & \tilde{\theta} & -(\tilde{\gamma}_q+\tilde{\delta}_q) \end{bmatrix}.$$

The DFE is locally asymptotically stable if all eigenvalues of this Jacobian have negative real parts, which holds when $\mathcal{R}_0 < 1$. The roots of the following cubic equation represent the eigenvalues of the Jacobian matrix J at the DFE:

$$(-\tilde{\sigma}-\lambda)(\tilde{\theta}+1+\tilde{\delta}+\lambda)(\tilde{\gamma}_q+\tilde{\delta}_q+\lambda)+\tilde{\beta}(1-\eta)\tilde{\sigma}(\tilde{\gamma}_q+\tilde{\delta}_q+\lambda)+\tilde{\beta}(1-\eta)\xi\tilde{\sigma}\tilde{\theta}=0.$$

According to the Routh-Hurwitz criterion and next-generation matrix theory, all roots λ have negative real parts when $\mathcal{R}_0 < 1$, ensuring that the DFE is locally asymptotically stable.
Numerically computed eigenvalues are represented as $a_1 = -1.5125$, $a_2 = -0.1717$, and $a_3 = -0.4158$, implying that the DFE is locally asymptotically stable.

3.7. Endemic equilibrium (for $\mathcal{R}_0 > 1$)

For the basic reproduction number satisfying $\mathcal{R}_0 > 1$, the system admits an endemic equilibrium characterized by the following expressions:

$$\begin{aligned} e^* &= \frac{(\tilde{\theta}+1+\tilde{\delta})}{\tilde{\sigma}} i^*, \\ q^* &= \frac{\tilde{\theta}}{\tilde{\gamma}_q+\tilde{\delta}_q} i^*, \\ r^* &= \frac{i^*}{\tilde{\omega}}\left(1+\frac{\tilde{\gamma}_q\tilde{\theta}}{\tilde{\gamma}_q+\tilde{\delta}_q}\right), \\ s^* &= \frac{(1-\eta)\tilde{\beta}(i^*+\xi q^*)}{\tilde{\nu}} v^*, \\ \tilde{\beta}(i^*+\xi q^*)\,(s^*+(1-\eta)v^*) &= (\tilde{\theta}+1+\tilde{\delta})i^*. \end{aligned}$$

Subject to the total population constraint $s^* + v^* + e^* + i^* + q^* + r^* = 1$, solving this system leads to a unique and biologically feasible endemic steady state, provided that $\mathcal{R}_0 > 1$. Numerically, we have $s* = 0.1199$, $v* = 0.3125$, $e* = 0.1199$, $i* = 0.0160$, $q* = 0.0160$, and $r* = 0.4157$, showing $\mathcal{R}_0 > 1$.

3.8. Global stability using a Lyapunov function

To examine the global stability, we construct a suitable Lyapunov function for the subsystem governing the infected compartments. Specifically, we consider the exposed (e), infectious (i), and quarantined (q) compartments, governed by the following equations:

$$\frac{de}{d\tau} = \tilde{\beta}(1-\eta)(i+\xi q) - \tilde{\sigma}e, \tag{3.7}$$

$$\frac{di}{d\tau} = \tilde{\sigma}e - (\tilde{\theta}+1+\tilde{\delta})i, \tag{3.8}$$

$$\frac{dq}{d\tau} = \tilde{\theta}i - (\tilde{\gamma}_q + \tilde{\delta}_q)q. \tag{3.9}$$

We define a Lyapunov function as a linear combination of the infected compartments

$$V(e,i,q) = a_1 e + a_2 i + a_3 q, \tag{3.10}$$

where the constants $a_1, a_2, a_3 > 0$ are to be determined. Differentiating V with respect to τ along the trajectories of the system, we obtain

$$\begin{aligned}\frac{dV}{d\tau} &= a_1\frac{de}{d\tau} + a_2\frac{di}{d\tau} + a_3\frac{dq}{d\tau}\\ &= a_1\left[\tilde{\beta}(1-\eta)(i+\xi q) - \tilde{\sigma}e\right] + a_2\left[\tilde{\sigma}e - (\tilde{\theta}+1+\tilde{\delta})i\right] + a_3\left[\tilde{\theta}i - (\tilde{\gamma}_q+\tilde{\delta}_q)q\right].\end{aligned} \tag{3.11}$$

To simplify and eliminate the cross-terms, we select

$$a_2 = a_1, \quad a_3 = \frac{a_1\tilde{\beta}(1-\eta)\xi}{\tilde{\gamma}_q + \tilde{\delta}_q}. \tag{3.12}$$

After some calculations, we derive

$$\frac{dV}{d\tau} = a_1 i(\mathcal{R}_0 - 1)(\tilde{\theta}+1+\tilde{\delta}). \tag{3.13}$$

Since $a_1 > 0$ and all parameters are non-negative, it follows that $\frac{dV}{d\tau} \leq 0$ whenever $\mathcal{R}_0 < 1$.
By LaSalle's invariance principle [22], we conclude that the DFE is globally asymptotically stable in the feasible region provided that $\mathcal{R}_0 < 1$. Therefore, controlling $\mathcal{R}_0$ below 1 ensures the eventual elimination of the disease.

4. Numerical simulations

We simulate the model using both the fourth-order Runge-Kutta method and MATLAB's built-in ode45. Parameters are selected from empirical literature or assumed within realistic bounds. Figures 2–9 show the evolution of compartments over time for various values of θ, η, and β.

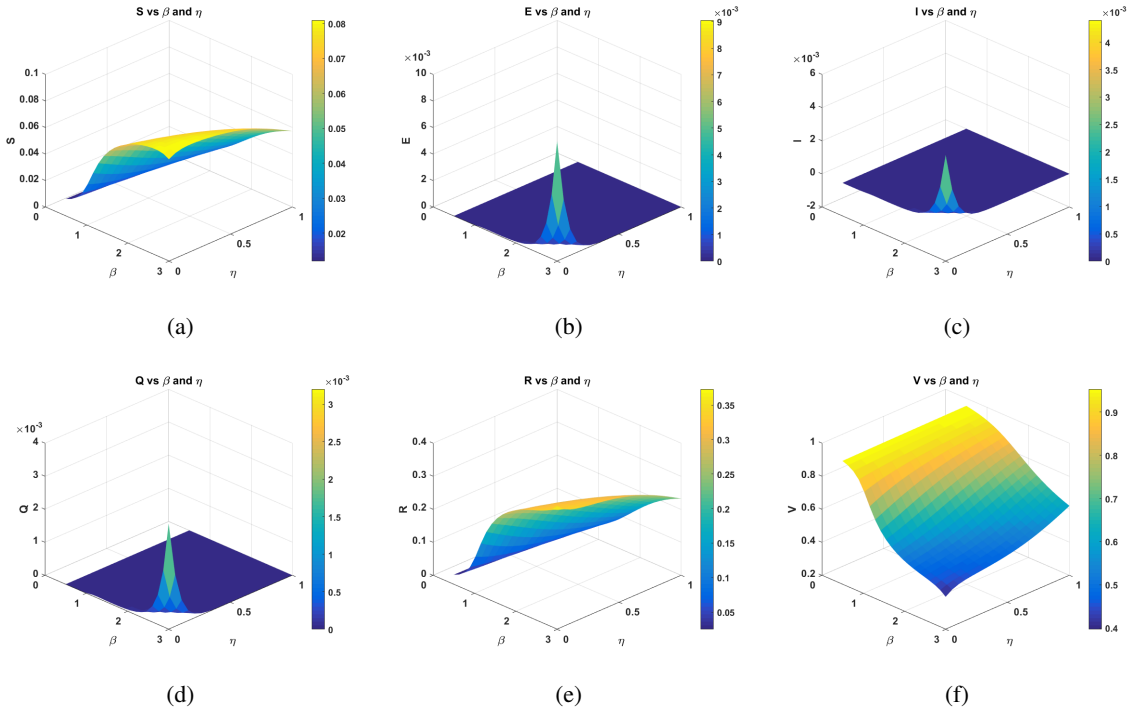

(a) (b) (c)

(d) (e) (f)

Figure 2. S, E, I, Q, R, and V versus β and η.

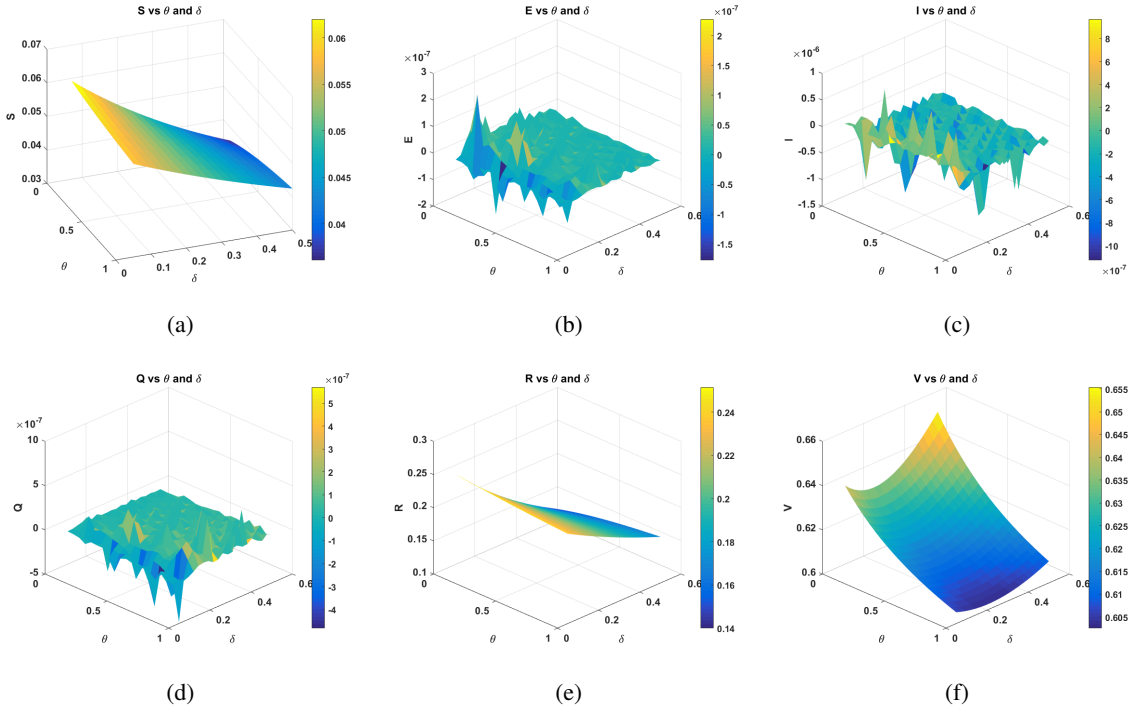

(a) (b) (c)

(d) (e) (f)

Figure 3. S, E, I, Q, R, and V versus θ and δ.

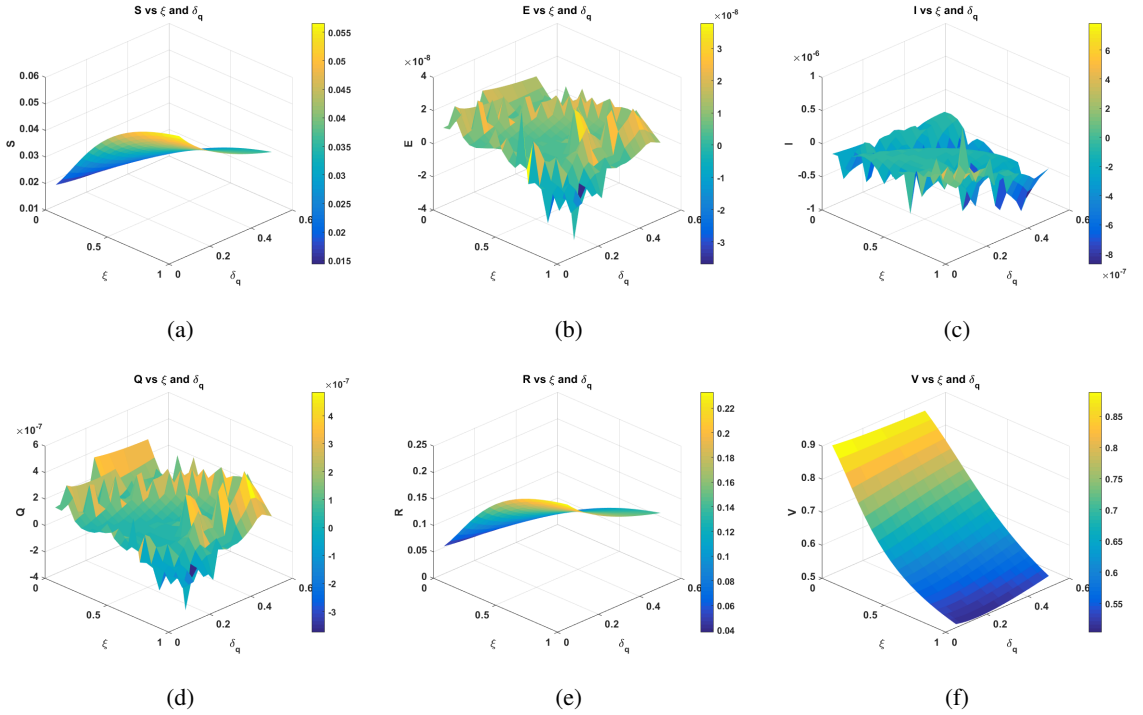

Figure 4. S, E, I, Q, R, and V versus ξ and δ_q.

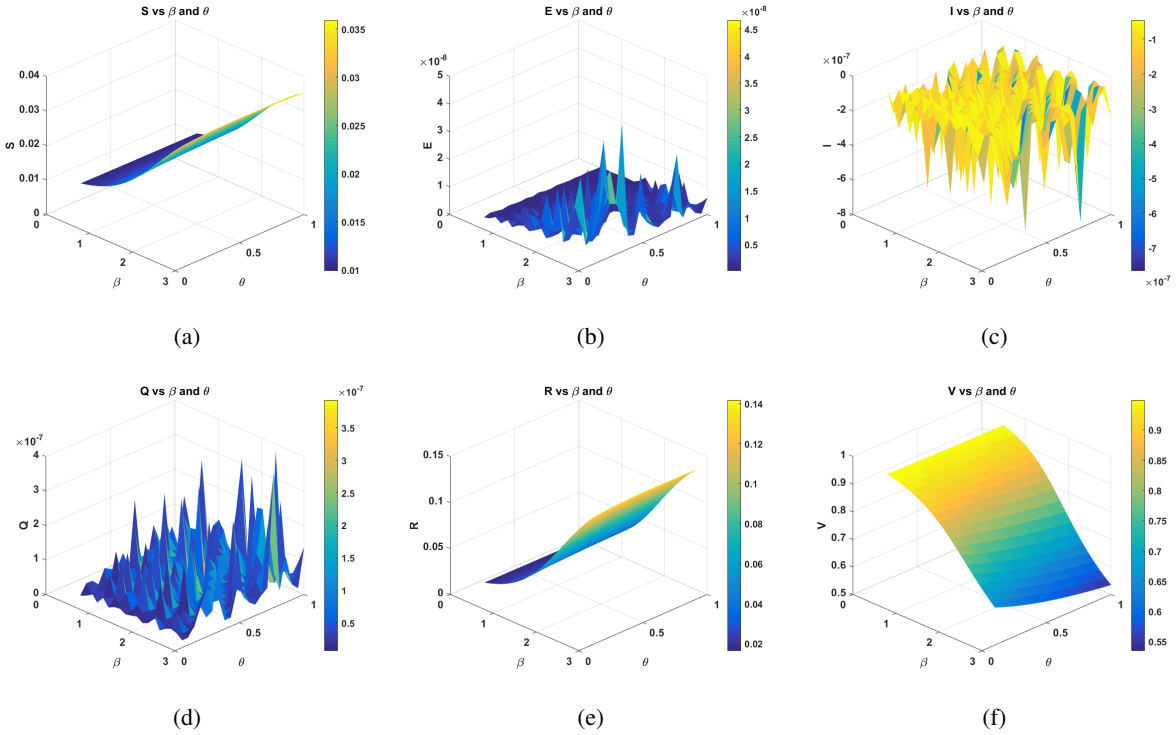

Figure 5. S, E, I, Q, R, and V versus β and θ.

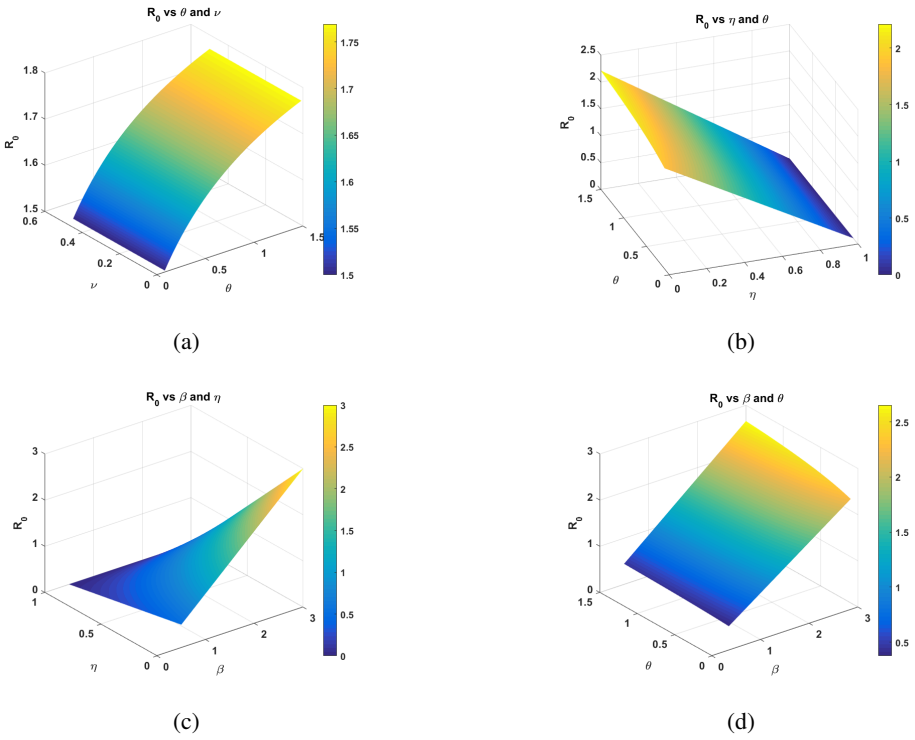

Figure 6. Surface plots of $\mathcal{R}_0$ versus the effective parameters.

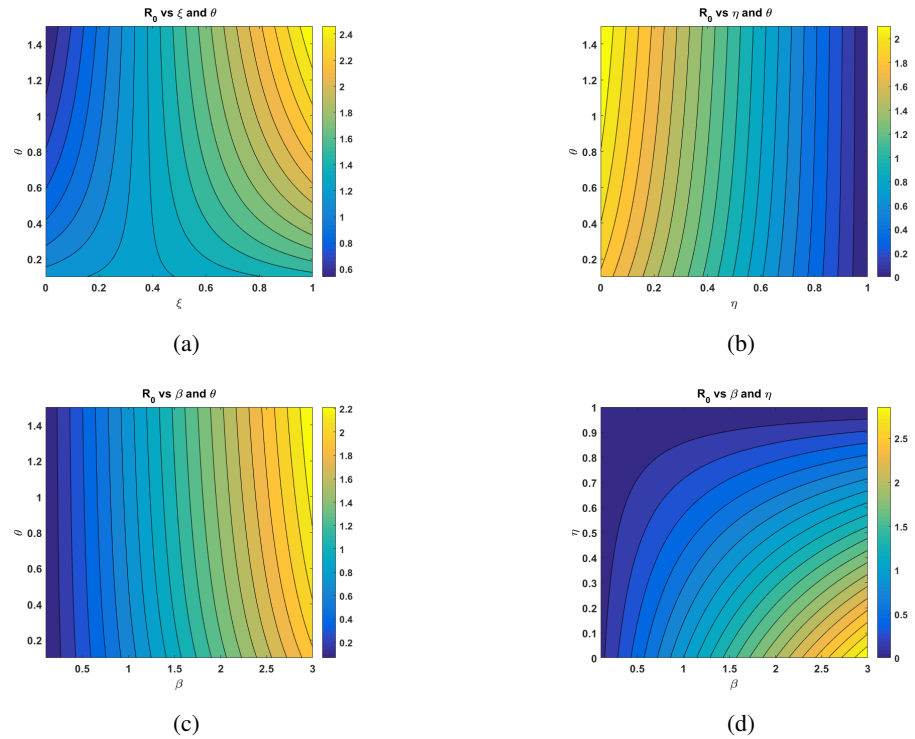

Figure 7. Contour plots of $\mathcal{R}_0$ versus the effective parameters.

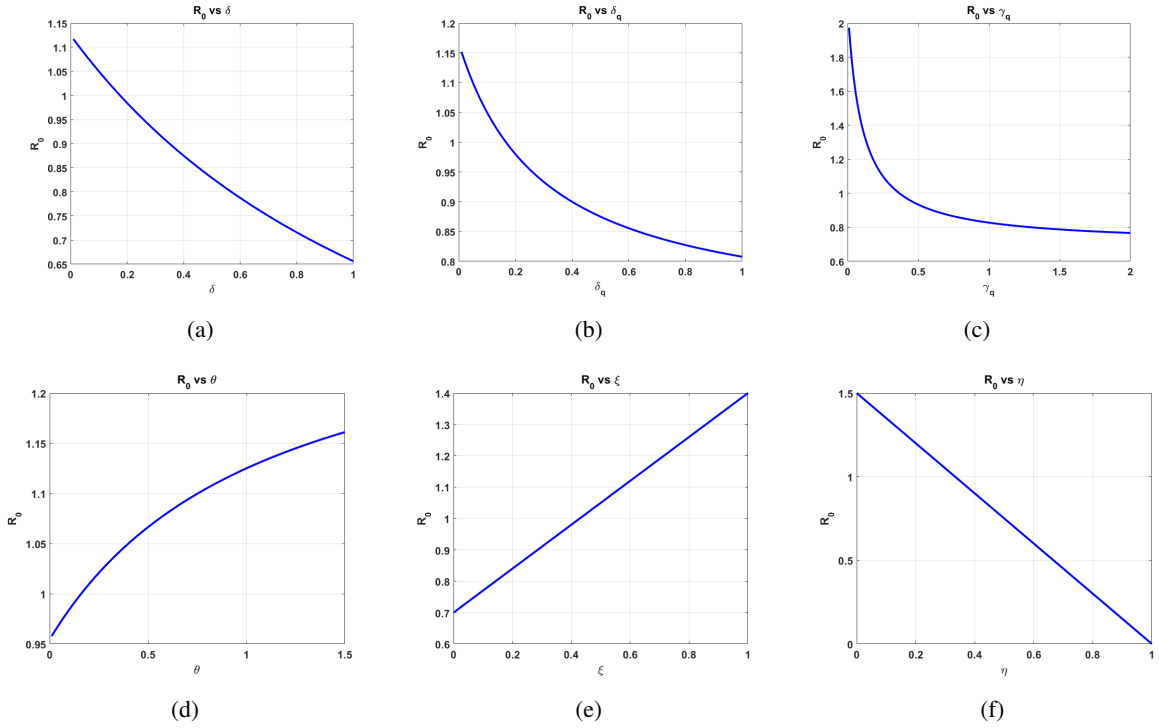

Figure 8. Line plots of $\mathcal{R}_0$ versus various parameters.

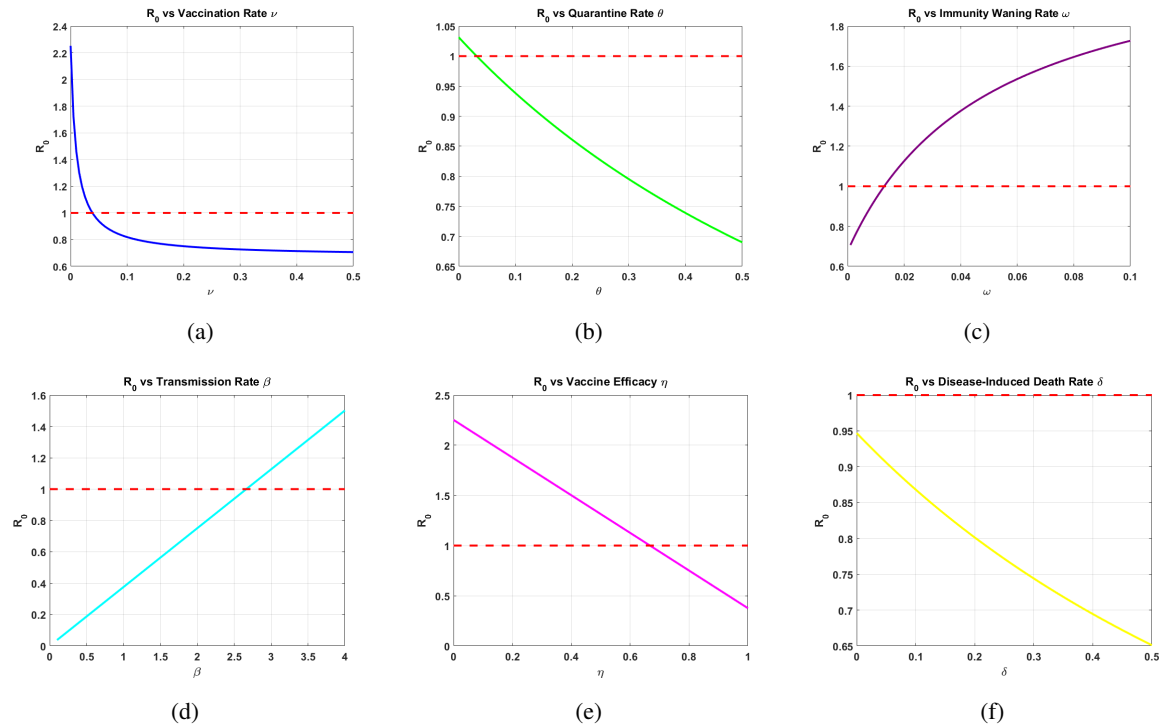

Figure 9. Threshold analysis of $\mathcal{R}_0$ versus various parameters.

The behavioral shifts in the population compartments during an endemic phase where $\mathcal{R}_0 < 1$ are

shown in Figure 10.

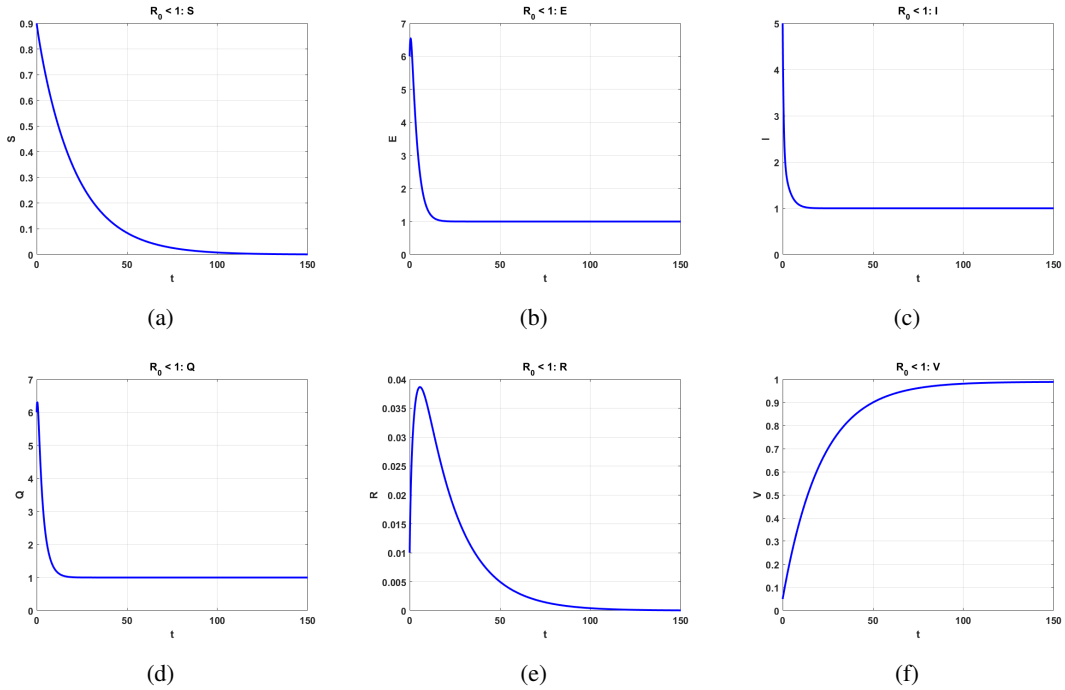

Figure 10. Dynamics of the population over time t when $\mathcal{R}_0 < 1$.

The behavioral shifts in the population compartments during pandemic phase where $\mathcal{R}_0 > 1$ are shown in Figure 11.

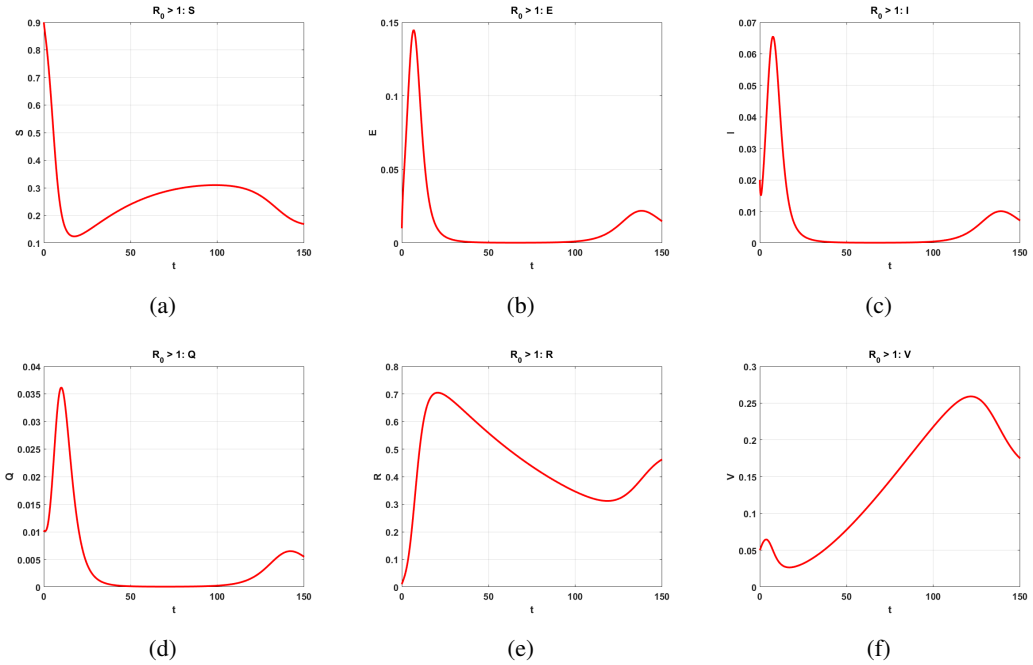

Figure 11. Dynamics of the population over time t when $\mathcal{R}_0 > 1$.

The behavioral shifts in the population compartments with variation of various parameters are shown in Figures 12–18.

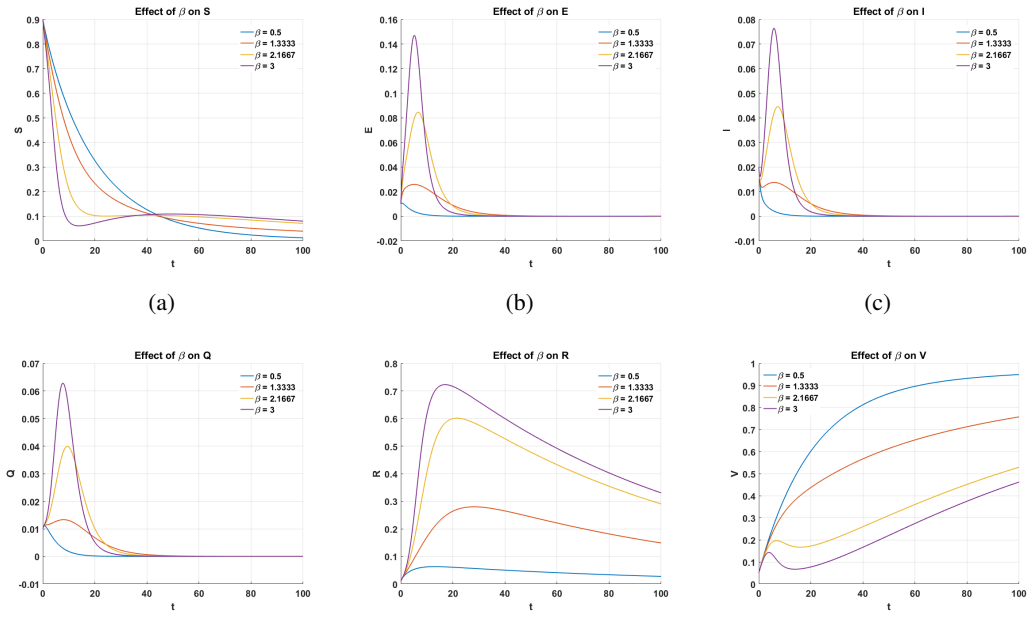

Figure 12. Dynamics of the population over time t against different values of β.

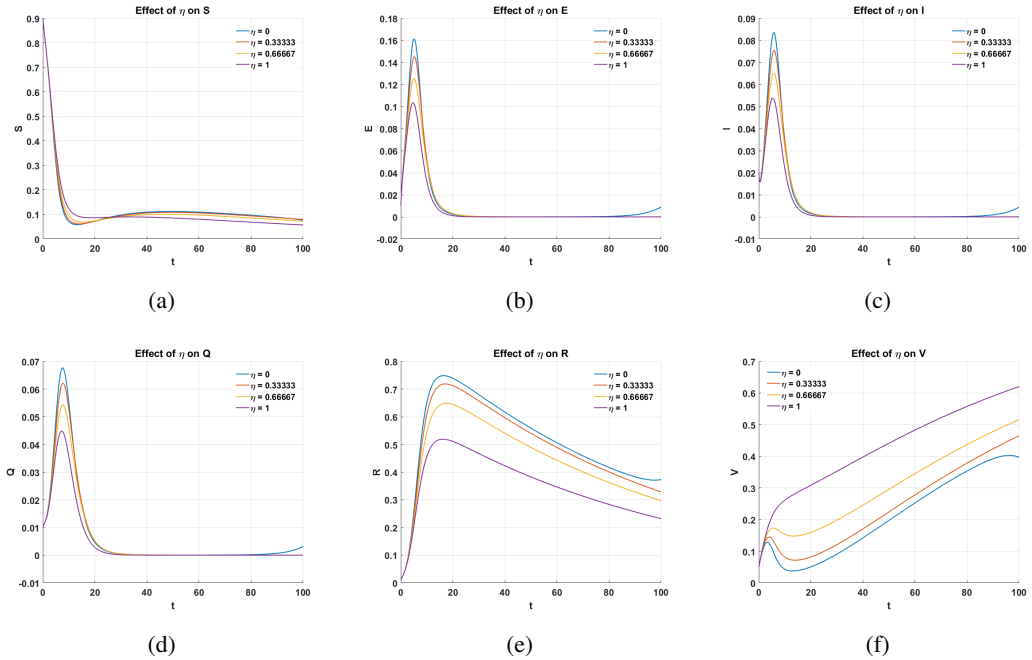

Figure 13. Dynamics of the population over time t against different values of η.

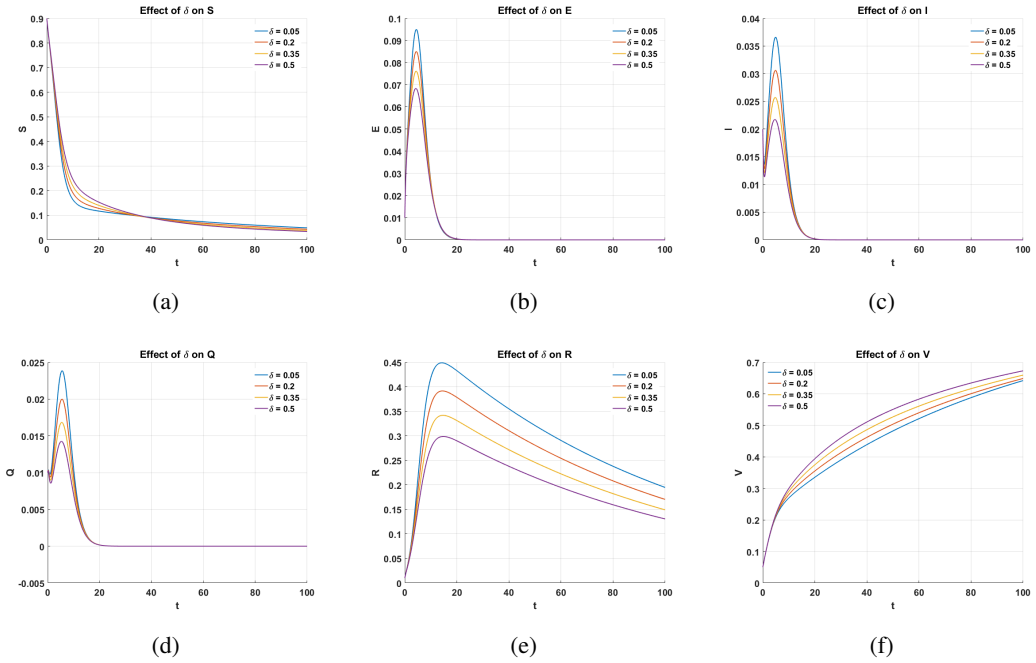

Figure 14. Dynamics of the population over time t against different values of δ.

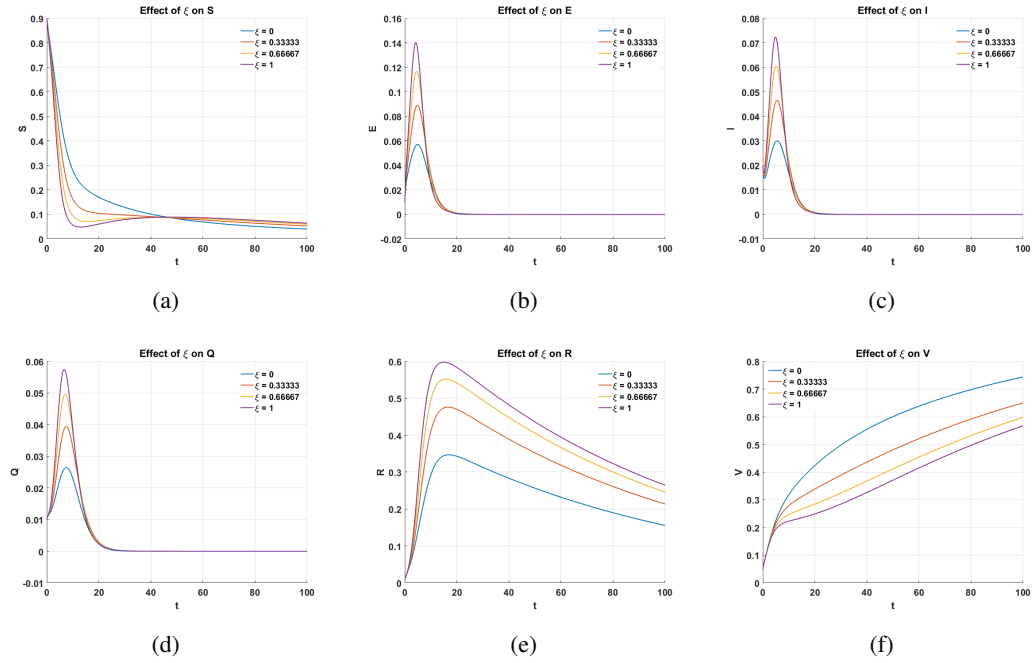

Figure 15. Dynamics of the population over time t against different values of ξ.

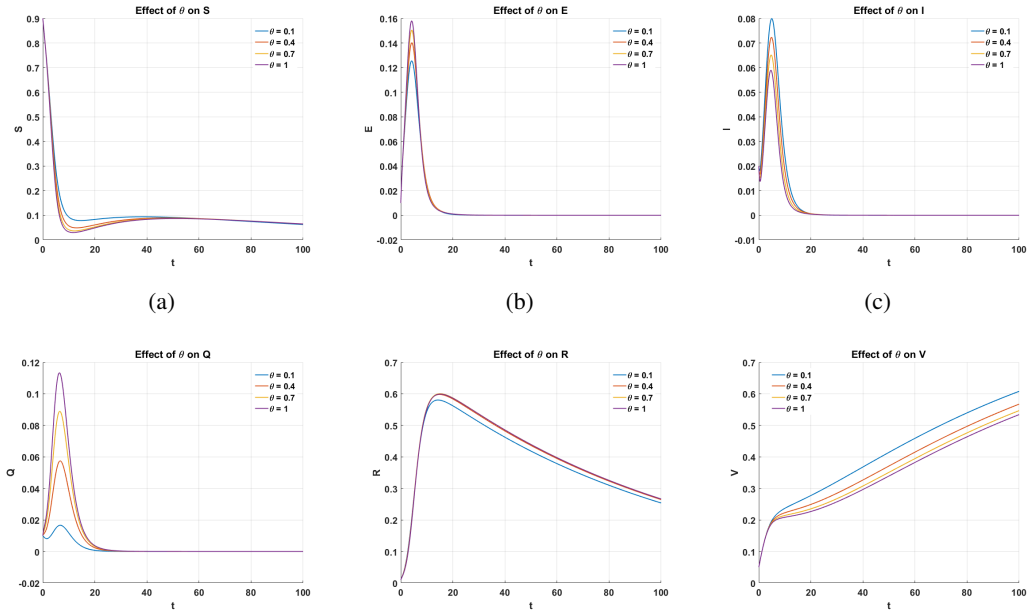

Figure 16. Dynamics of the population over time t against different values of θ.

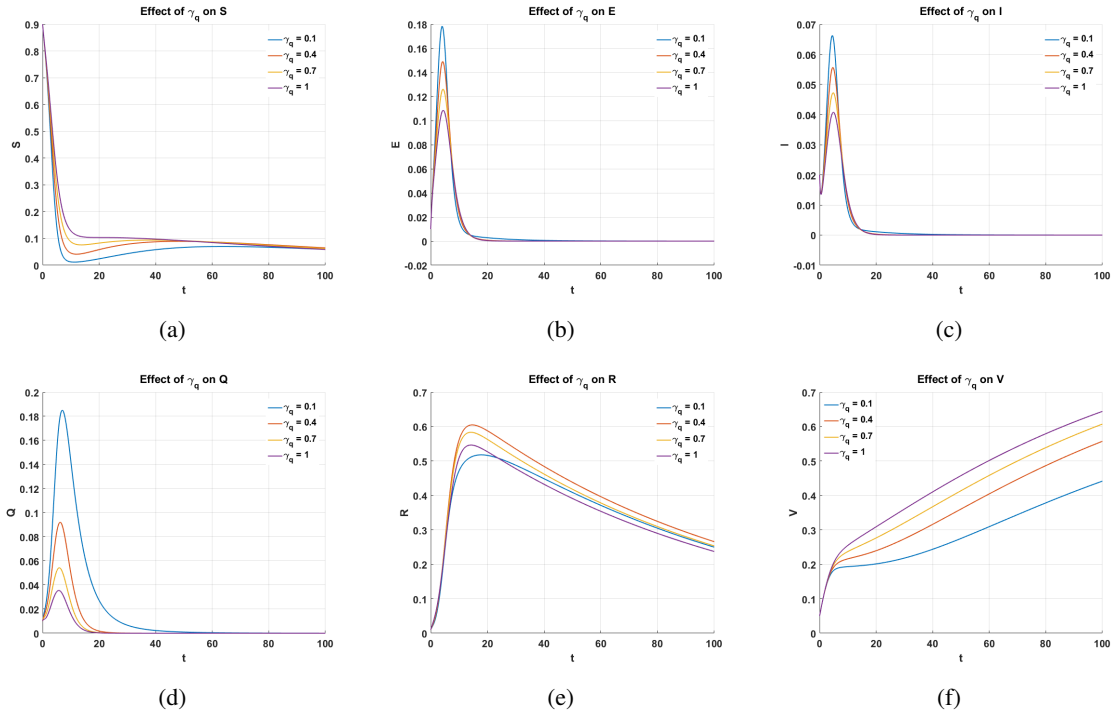

Figure 17. Dynamics of the population over time t against different values of γ_q.

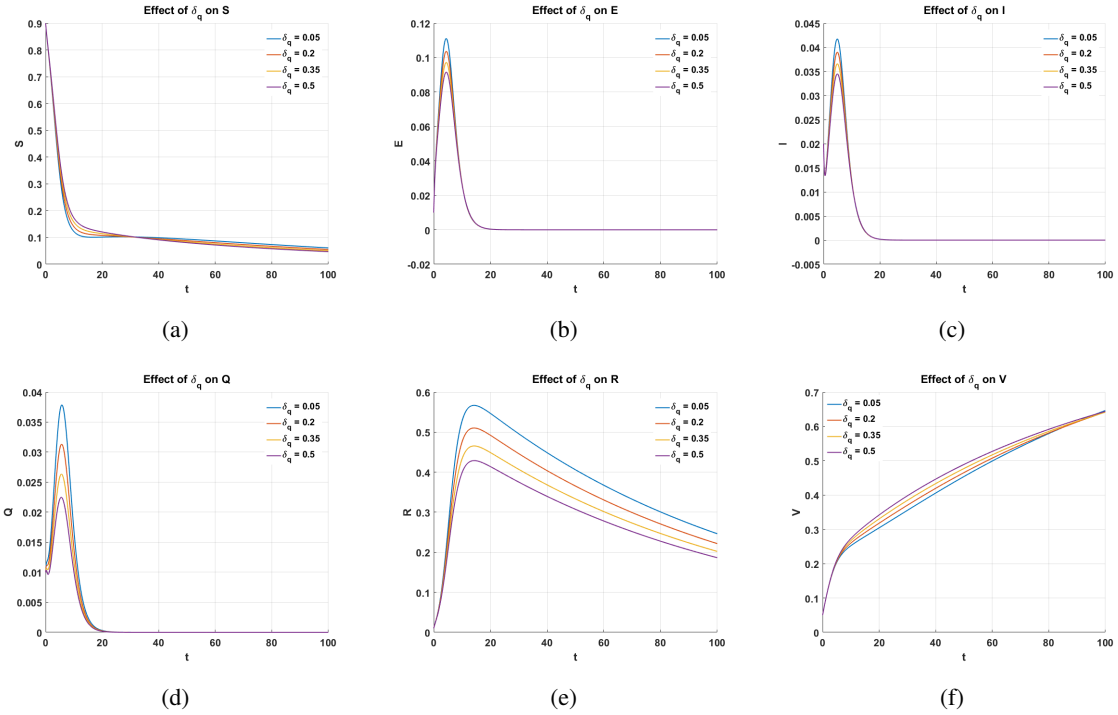

Figure 18. Dynamics of the population over time t against different values of δ_q.

4.1. Sensitivity analysis

To evaluate the influence of various parameters on the basic reproduction number $\mathcal{R}_0$, we utilize the normalized forward sensitivity index, defined by

$$\Gamma_p = \frac{\partial \mathcal{R}_0}{\partial p} \cdot \frac{p}{\mathcal{R}_0},$$

where p denotes a given model parameter. This index quantifies the proportional change in $\mathcal{R}_0$ resulting from a proportional change in p.

Parameters such as the transmission rate $\tilde{\beta}$, the vaccination rate $\tilde{\nu}$, and the vaccine efficacy η exhibit high sensitivity values, suggesting that they play a crucial role in shaping the epidemic dynamics and are key targets for intervention strategies.

Below, we list the explicit expressions for the normalized forward sensitivity indices of $\mathcal{R}_0$ with respect to each parameter.

- Sensitivity of $\mathcal{R}_0$ with respect to $\tilde{\beta}$:

$$\Gamma_{\tilde{\beta}}^{\mathcal{R}_0} = 1.$$

- Sensitivity of $\mathcal{R}_0$ with respect to η:

$$\Gamma_{\eta}^{\mathcal{R}_0} = \frac{\eta}{\eta - 1}.$$

- Sensitivity of $\mathcal{R}_0$ with respect to ξ:

$$\Gamma_{\xi}^{\mathcal{R}_0} = \frac{\theta\xi}{\delta_q + \gamma_q + \theta\xi}.$$

- Sensitivity of $\mathcal{R}_0$ with respect to σ:

$$\Gamma_{\sigma}^{\mathcal{R}_0} = 0.$$

- Sensitivity of $\mathcal{R}_0$ with respect to θ:

$$\Gamma_{\theta}^{\mathcal{R}_0} = -\frac{\theta(\delta_q + \gamma_q - \xi - \delta\xi)}{(\delta + \theta + 1)(\delta_q + \gamma_q + \theta\xi)}.$$

- Sensitivity of $\mathcal{R}_0$ with respect to δ:

$$\Gamma_{\delta}^{\mathcal{R}_0} = -\frac{\delta}{\delta + \theta + 1}.$$

- Sensitivity of $\mathcal{R}_0$ with respect to γ_q:

$$\Gamma_{\gamma_q}^{\mathcal{R}_0} = -\frac{\gamma_q\theta\xi}{(\delta_q + \gamma_q)(\delta_q + \gamma_q + \theta\xi)}.$$

- Sensitivity of $\mathcal{R}_0$ with respect to δ_q:

$$\Gamma_{\delta_q}^{\mathcal{R}_0} = -\frac{\delta_q\theta\xi}{(\delta_q + \gamma_q)(\delta_q + \gamma_q + \theta\xi)}.$$

- Sensitivity of $\mathcal{R}_0$ with respect to ν:

$$\Gamma_{\nu}^{\mathcal{R}_0} = 0.$$

- Sensitivity of $\mathcal{R}_0$ with respect to ω:

$$\Gamma_{\omega}^{\mathcal{R}_0} = 0.$$

Figures 19 and 20 illustrate the computed normalized forward sensitivity indices and partial rank correlation coefficient (PRCC) sensitivity indices for each parameter in the model, respectively.

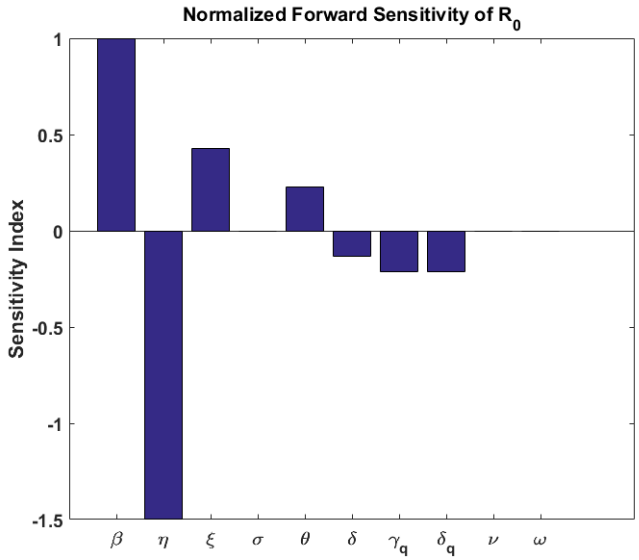

Figure 19. Sensitivity analysis.

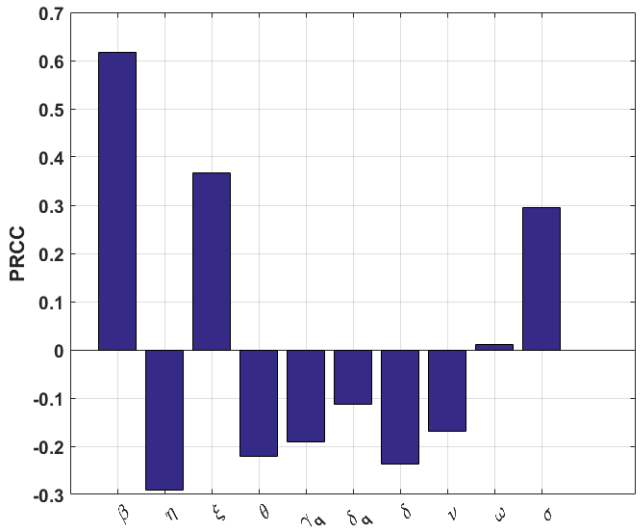

Figure 20. Partial rank correlation coefficient (PRCC) of the model's output to the parameters.

Table 3 presents the sensitivity of the model with respect to variations in the key model parameters.

Table 3. Normalized forward sensitivity indices and interpretations of $\mathcal{R}_0$.

Parameter	Γ_p	Interpretation
$\tilde{\beta}$	1	Linear effect: A 10% increase in $\tilde{\beta}$ results in a 10% increase in $\mathcal{R}_0$.
η	$\frac{\eta}{\eta - 1}$	Negative influence: As vaccine efficacy η rises, $\mathcal{R}_0$ declines.
ξ	$\frac{\theta\xi}{\tilde{\gamma}_q + \tilde{\delta}_q + \theta\xi}$	Positive effect: Higher infectiousness of quarantined individuals elevates $\mathcal{R}_0$.
$\tilde{\sigma}$	0	No direct impact on $\mathcal{R}_0$; it does not appear explicitly in the formula.
$\tilde{\theta}$	*Complex*	Effect depends on the interplay with ξ; increasing the quarantine rate can raise or lower $\mathcal{R}_0$.
$\tilde{\delta}$	$-\frac{\delta}{\delta + \theta + 1}$	Negative contribution: Greater recovery or death among infected individuals reduces $\mathcal{R}_0$.
$\tilde{\gamma}_q$	*Negative*	Faster recovery in quarantine helps diminish disease spread, lowering $\mathcal{R}_0$.
$\tilde{\delta}_q$	*Negative*	Higher mortality or removal in quarantine lessens the transmission potential.
$\tilde{\nu}, \tilde{\omega}$	0	These parameters do not affect $\mathcal{R}_0$ directly; they influence the long-term behavior of the system rather than early outbreak potential.

5. Discussion of numerical results

This section provides a detailed analysis of the numerical simulations shown in Figures 2–20, highlighting the dynamics of disease transmission and assessing the effectiveness of various control measures within the context of the NB.1.8.1 COVID-19 variant.

Figures 2–5 depict the temporal evolution of all six compartments over the infection transmission rate, vaccine efficacy, and isolation. Figure 2 explores the joint effects of the transmission rate β

and vaccine efficacy η on the model's compartments. As shown in Figure 2(a), an increase in β results in a significant reduction in the susceptible population due to higher infection rates, while greater η values reduce this effect by limiting transmission through more effective vaccination. In Figures 2(b)–(d), the exposed, infected, and quarantined populations grow with increased β, especially when η is low, confirming that ineffective vaccines allow for more disease spread. Figure 2(e) shows that the recovered population increases with higher values of individuals going through the infection and recovery process. Lastly, Figure 2(f) illustrates that the vaccinated population grows with increased vaccine efficacy, as more individuals are successfully protected. This figure collectively illustrates how improved vaccine effectiveness and transmission control can significantly influence the epidemic's containment. It highlights the importance of timely and effective vaccination in decreasing the transmission potential of highly infectious variants. This aligns with the biological understanding that higher transmission rates lead to more individuals being exposed in a shorter period. These findings emphasize the need for strategies aimed at reducing β, such as physical distancing, wearing face masks, and limiting large gatherings, especially during the early stages of an outbreak or when highly transmissible variants are present. Quarantine measures help lower the infectious load. Over time, the classes of recovered and vaccinated individuals become predominant, indicating a shift toward effective containment and control of the disease. However, these figures show that vaccines with higher efficacy reduce exposure risk by enhancing immune protection in the vaccinated population.

Figure 3 presents the combined effect of the quarantine rate θ and the disease-induced mortality rate δ on the compartmental dynamics. Figure 3(a) shows that the susceptible population grows with a higher θ, as infected individuals are removed more quickly, reducing further exposure. Figure 3(b)–(d) demonstrates a decrease in the exposed, infectious, and quarantined groups as θ and δ increase, indicating that effective isolation and natural disease progression limit the spread. Oscillations in Figure 3(b)–(d) are particularly evident at moderate quarantine levels, showing unstable intermediate dynamics before stabilizing. Figure 3(e) indicates that the recovered population rises with θ, thanks to timely intervention and isolation. Meanwhile, the vaccinated population in Figure 3(f) slightly improves with higher quarantine rates but drops when mortality is high, implying that severe outcomes reduce the effectiveness of long-term public health measures. These plots highlight the crucial role of timely isolation and disease severity in shaping epidemic outcomes, emphasizing how isolation and clinical factors like mortality can strongly influence the outbreak's course and control efforts strategies.

Figure 4 illustrates the interaction between the level of infectiousness of quarantined individuals (ξ) and the death rate within quarantine (δ_q). Figure 4(a) shows that the susceptible class stays higher when it ξ is low and δ_q is higher, as effective isolation and fatalities prevent onward transmission. Figure 4(b)–(d) demonstrates that higher ξ values destabilize the exposed, infected, and quarantined groups, allowing infections to persist even with isolation. In contrast, increasing δ_q reduces these groups by removing individuals more quickly from the epidemic cycle. Figure 4(e) shows that the recovered group initially grows with moderate ξ, but declines at high δ_q levels due to fewer surviving cases. Lastly, Figure 4(f) indicates that vaccination plays a limited role in this scenario but slightly decreases with rising ξ, reflecting the indirect effects of persistent infections on vaccine-driven protection. This highlights the importance of strict quarantine enforcement and reducing contact between isolated and susceptible populations.

Figure 5 explores how changing the transmission rate β and the quarantine rate θ together influence disease dynamics. From Figure 5(a), it is clear that increasing θ helps protect the susceptible

population, while raising β leads to a decline due to greater exposure. Figure 5(b)–(d) confirms that higher transmission rates increase the exposed, infectious, and quarantined populations, while effective quarantine reduces this growth. Notably, the infected curve reacts more strongly to β, and quarantine lessens the infectious load by diverting people from active spread. Figure 5(e) shows that recovery rates rise with both parameters, as more individuals recover naturally or through quarantine. Figure 5(f) indicates a slight increase in vaccination coverage with rising θ, while higher β indirectly suppresses vaccination by speeding up infection. This figure demonstrates the delicate balance between transmission and isolation measures in controlling the disease outbreak.

Figure 6 illustrates how the basic reproduction number ($\mathcal{R}_0$) varies with different pairs of model parameters. In Figure 6(a), the interaction between the vaccination rate ν and the quarantine rate θ is examined. The plot shows that increasing both parameters simultaneously results in a significant decline in $\mathcal{R}_0$, highlighting the combined effectiveness of the vaccination and isolation strategies. Figure 6(b) explores the influence of vaccine efficacy η and the quarantine rate θ, revealing that high efficacy paired with a effective quarantine strategy greatly reduces disease transmission. In Figure 6(c), the surface plot of the transmission rate β and vaccine efficacy η shows that while high transmission increases $\mathcal{R}_0$; this effect can be counteracted by deploying highly effective vaccines. Figure 6(d) investigates the impact of the transmission rate β along with the quarantine rate θ, confirming that even with increased transmissibility, stringent quarantine efforts can reduce it $\mathcal{R}_0$ to manageable levels.

Figure 7 provides two-dimensional contour plots for selected parameter pairs, offering a clearer view of where $\mathcal{R}_0$ is below or above the threshold of 1. In Figure 7(a), the contour lines show that decreasing the infectiousness of quarantined individuals (ξ) while increasing the quarantine rate θ keeps $\mathcal{R}_0$ suppressed. Figure 7(b) supports the idea that higher vaccine efficacy η and better isolation help control the disease. Figure 7(c) demonstrates that the negative effects of a high transmission rate β can be reduced through enough quarantine, and Figure 7(d) further highlights that combining vaccine efficacy with reduced transmission is essential for disease management. Overall, the contour plots give valuable insights into parameter combinations that ensure $\mathcal{R}_0 < 1$.

Figure 8 presents a series of line plots that analyze how $\mathcal{R}_0$ varies with individual parameters while keeping others constant. In Figure 8(a), it is evident that an increase in the death rate of infectious individuals (δ) causes a steady decrease in $\mathcal{R}_0$, since it shortens the infectious period. A similar pattern appears in Figure 8(b), where the death rate in quarantine (δ_q) also reduces the reproduction number. Figure 8(c) shows that increasing the recovery rate in the quarantined group (γ_q) has a positive impact by lowering $\mathcal{R}_0$. In Figure 8(d), the effect of the quarantine rate θ) emphasizes that more aggressive isolation strategies are effective in controlling the disease. Figure 8(e) demonstrates that as the infectiousness level of the quarantined population (ξ) increases, $\mathcal{R}_0$ also rises, highlighting that reducing contact or enhancing containment in quarantine is crucial. Lastly, Figure 8(f) indicates that higher vaccine efficacy η consistently decreases $\mathcal{R}_0$, underscoring the importance of effective immunization programs.

Figure 9 explores the threshold dynamics of $\mathcal{R}_0$ by plotting it against several critical control parameters, with a red dashed line marking the epidemic threshold at $\mathcal{R}_0 = 1$. In Figure 9(a), increasing the vaccination rate ν results in a rapid decline in $\mathcal{R}_0$, with values falling below one at relatively low vaccination levels, emphasizing the high effectiveness of immunization. Figure 9(b) reveals a similar trend with the quarantine rate θ; modest increases are sufficient to bring the reproduction number below one. Figure 9(c) shows the impact of a waning immunity rate ω, where higher values lead to a

resurgence of $\mathcal{R}_0$, indicating the risk of reinfection and the importance of booster doses. In Figure 9(d), the transmission rate β is directly proportional to $\mathcal{R}_0$, as expected. Figure 9(e) highlights that increasing vaccine efficacy η is effective in reducing $\mathcal{R}_0$ even when transmission remains high. Finally, Figure 9(f) shows that higher disease-induced mortality (δ) decreases the reproduction number, though this is not a desirable control mechanism from a public health standpoint.

Figures 10 and 11 compare situations where $\mathcal{R}_0 < 1$ and $\mathcal{R}_0 > 1$. When $\mathcal{R}_0 < 1$, the infection gradually dies out, leading to disease elimination. In contrast, $\mathcal{R}_0 > 1$ results in persistent infection levels, indicating endemicity. This critical threshold shows the tipping point between eradication and long-term circulation, guiding policy targets for transmission control.

Figures 12–18 highlight parameter variations and their effects on compartmental dynamics. Figure 12 shows how the transmission rate β affects the population compartments. As β increases, the susceptible class declines more quickly due to increased exposure, leading to a sharp increase in the exposed, infected, and quarantined populations. The infection peaks earlier and at a higher level with a larger β, indicating faster epidemic growth. The recovered population initially grows but later declines, possibly due to reinfection or waning immunity. The vaccinated group shows steady but modest growth, suggesting that vaccination coverage is still insufficient to fully counteract high transmission rates. In Figure 13, the effect of vaccine efficacy η is investigated. An increase in η leads to a significant reduction in the exposed and infected groups, emphasizing the importance of vaccine protection. The susceptible population decreases more gradually, while the vaccinated group increases notably as higher efficacy improves the immune response. At the same time, fewer individuals become quarantined or recover, since disease spread is more effectively controlled at the source. These findings highlight the need to improve vaccine efficacy to better reduce disease spread and lessen the healthcare burden. Figure 14 investigates the effect of varying the death rate δ among infectious individuals. As δ increases, the size of the infected compartment I decreases more rapidly due to increased mortality. This leads to a decline in secondary infections and a subsequent reduction in the exposed and quarantined populations. The recovered class slightly reduces, since more individuals die before recovering. The susceptible and vaccinated populations remain mostly unaffected by δ, indicating that this parameter chiefly impacts the disease progression of currently infected individuals. These dynamics emphasize the urgency of interventions that reduce fatality, such as improved clinical care and early detection.

Figure 15 illustrates the impact of varying ξ, which represents the level of infectiousness of quarantined individuals relative to those in the infectious class. As ξ increases, indicating that quarantined individuals are still capable of transmitting the disease at a higher rate, there is a noticeable rise in the exposed and infected compartments. This occurs because quarantine becomes less effective at interrupting transmission chains. Correspondingly, the susceptible population declines more rapidly due to the higher force of infection.

At higher values of ξ, the quarantined population initially grows but this measure is less effective at containing the spread, while the recovered group rises more slowly. The vaccinated compartment remains largely unchanged, as it is independent of direct disease transmission dynamics. These results underscore the critical importance of ensuring strict isolation and minimizing exposure during quarantine to keep ξ as low as possible, thereby enhancing the effectiveness of public health interventions. In Figure 16, the quarantine rate θ is varied to evaluate its effect on disease spread. A higher quarantine rate causes infectious individuals to move into quarantine more quickly, decreasing

the size of the infected group. The quarantined class shows sharper, earlier peaks at a higher θ, followed by faster declines as individuals recover. The exposed group also decreases due to fewer infectious contacts. Overall, these results emphasize the importance of implementing timely isolation policies to control the epidemic effectively. Figure 17 shows the effect of increasing the quarantine recovery rate γ_q. A higher γ_q means quarantined individuals recover more quickly, which shortens their quarantine duration and reduces the number of people in that compartment. This leads to more recovered individuals, while the exposed and infected groups decrease. Importantly, changing γ_q has little impact on the susceptible and vaccinated groups. These findings suggest that improving recovery in quarantine can indirectly lower disease prevalence and speed up the overall population recovery. Figure 18 examines how altering the death rate of quarantined individuals, represented by δ_q, affects disease dynamics. As δ_q increases, more quarantined individuals die instead of recovering. This leads to a decline in the quarantined population over time and slows the flow into the recovered group, which grows more gradually with higher δ_q. The infected and exposed groups may also be slightly impacted, showing minor decreases, because fewer individuals return from quarantine to contribute to transmission. Meanwhile, the susceptible and vaccinated groups remain relatively stable, as they are less affected by changes in quarantine outcomes. These findings emphasize the importance of reducing mortality in quarantine by providing better treatment, monitoring, and supportive care for individuals in isolation.

Figures 19 and 20 show global sensitivity analyses for the basic reproduction number $\mathcal{R}_0$. These figures indicate that the most sensitive parameters affecting $\mathcal{R}_0$ are the transmission rate β, vaccine efficacy η, and the quarantine infectivity factor ξ. This information helps policymakers focus on interventions that target these key factors, such as enhancing vaccine effectiveness, enforcing strict quarantine protocols, and minimizing contacts to effectively keep the reproduction number below 1.

Collectively, these figures support the conclusion that successful epidemic control requires a multifaceted approach that reduces transmission rates, maximizes vaccine efficacy, manages waning immunity, and implements efficient isolation protocols. The model's flexibility allows for real-time assessment of various public health strategies under different assumptions, making it a valuable tool for ongoing pandemic responses and preparedness for future variants.

6. Conclusions

In this study, we presented a novel SEIR-VQ model specifically developed to capture the transmission dynamics of the NB.1.8.1 variant of COVID-19. The model highlights key features, including partial vaccine protection, waning immunity over time, quarantine measures, breakthrough infections, and a time-dependent transmission rate. These critical real-world features make the model highly relevant for understanding the behavior of emerging variants under realistic public health and epidemiological conditions situations.

By proving the positivity and boundedness of all compartments, we established the mathematical well-posedness of the model. Using the next-generation matrix approach, we derived the basic reproduction number $\mathcal{R}_0$. We then employed a Lyapunov function to demonstrate that the disease-free equilibrium is globally asymptotically stable when $\mathcal{R}_0 < 1$. The model also admits an endemic equilibrium when $\mathcal{R}_0 > 1$, suggesting that continued transmission may occur if key control parameters are not effectively managed implemented.

The numerical simulations, conducted using both the classical Runge-Kutta method and MATLAB's ode45 solver, highlighted the following key observations:

- Figures 2–5 demonstrate that increasing the transmission rate β or decreasing the vaccine's efficacy η results in a sharp rise in infections. Conversely, higher vaccination coverage and a greater isolation rate θ significantly decrease the infectious population.
- Figures 6–9 depict how different parameters influence $\mathcal{R}_0$. Surface and contour plots reveal that combinations of high β and low η push $\mathcal{R}_0$ above 1, while effective vaccination and quarantine measures keep it below the epidemic threshold.
- Figures 10 and 11 confirm that when $\mathcal{R}_0 < 1$, all infectious compartments tend toward zero over time, indicating disease eradication. When $\mathcal{R}_0 > 1$, the infection persists, highlighting the importance of timely and effective intervention strategies.
- Figures 12–18 examine the system's response to changes in the parameters. These results stress that isolating infectious individuals and enhancing vaccine efficacy are among the most effective strategies.
- In Figures 19 and 20, sensitivity analysis identified β, ξ, and η as the most influential parameters on $\mathcal{R}_0$, suggesting these should be the primary targets for public health efforts to reduce transmission.

The simulation results provide biologically meaningful insights into the NB.1.8.1 variant's dynamics, especially under the influence of partial vaccination, waning immunity, and reinfection. The model shows how even vaccinated or recovered individuals can re-enter the susceptible pool over time, leading to prolonged transmission. It also demonstrates that imperfect quarantine can still allow some spread, consistent with real-world observations. Overall, the findings emphasize that controlling such an evolving virus requires a combination of timely vaccination, isolation, and booster strategies to reduce both susceptibility and exposure risks.

The proposed numerical simulations employ the classical RK4 method along with MATLAB's ode45 solver, delivering both accuracy and computational efficiency. The RK4 scheme offers highly stable and precise solutions for nonlinear systems, making it suitable for modeling complex epidemic dynamics with time-varying parameters. Meanwhile, MATLAB solvers such as `ode45` further improve flexibility by automatically adjusting step sizes, ensuring robust performance even in stiff or sensitive regions of the solution.

Our findings suggest that controlling NB.1.8.1 requires a combination of high vaccination coverage and strong isolation policies, especially in situations where reinfection and breakthrough infections are common. The study shows that vaccination alone cannot control the epidemic unless its efficacy is significantly high. Even moderate vaccine efficacy may still lead to outbreaks if not combined with isolation and other measures to reduce transmission. The model provides strong numerical and theoretical evidence that the NB.1.8.1 variant can be effectively controlled if infectious individuals are quickly isolated and if high vaccine coverage and efficacy are maintained. The model's flexibility also makes it a well-suited and potentially valuable tool for evaluating public health policies in response to emerging viral variants.

To enhance the scope and potential applications of the model; the following directions are suggested for future research:

- Generalizing the model to include various age groups and booster immunizations;

- introducing fractional-order derivatives or time delays to model behavioral memory and incubation;
- integrating real-world epidemiological data for the NB.1.8.1 to enhance the model's predictive performance;
- introducing stochastic elements and regional variability to better capture localized outbreaks and uncertainty.

These extensions will enhance the model's adaptability, realism, and utility in guiding public health responses to future COVID-19 variants and other infectious diseases.

Author contributions

Faiza Arif: Writing-original draft, software, formal analysis, data curation; Sana Ullah Saqib: Writing-original draft, software, formal analysis, data curation, review and editing, methodology, visualization; Yin-Tzer Shih: Conceptualization, writing-review and editing, supervision; Aneela Kausar: Writing-original draft, software, investigation, review and editing, methodology, visualization, supervision. All authors have read and approved the final version of the manuscript for publication.

Use of Generative-AI tools declaration

The authors declare that they have not used artificial intelligence (AI) tools in the creation of this article.

Acknowledgments

The authors would like to thank the anonymous referees for their kind comments and valuable suggestions.

The authors gratefully acknowledge the support of the National Science and Technology Council (NSTC), Taiwan, through the NSTC project under Grant No. NSTC 114-2115-M-005-002-MY2.

Conflict of interest

The authors declare that they have no conflict of interest regarding the publication of this paper.

References

1. H. W. Hethcote, The mathematics of infectious diseases, *SIAM Rev.*, **42** (2000), 599–653. https://doi.org/10.1137/S0036144500371907
2. H. Hukmah, M. R. Nisardi, S. Sulma, Mathematical model of COVID-19 with quarantine and vaccination, *J. Mat. Statistika Komputasi*, **19** (2023), 266–285. https://doi.org/10.20956/j.v19i2.22301

3. A. Zeb, S. M. Alzahrani, A. Z. Alshahrani, N. Erturk, M. A. Zaman, Mathematical modeling and analysis of COVID-19 in Pakistan, *Chaos Soliton. Fract.*, **138** (2020), 109949. https://doi.org/10.1016/j.chaos.2020.109949
4. S. Y. Tchoumi, H. Rwezaura, J. M. Tchuenche, Dynamic of a two-strain COVID-19 model with vaccination, *Results Phys.*, **39** (2022), 105777. https://doi.org/10.1016/j.rinp.2022.105777
5. S. Chatterjee, A. N. Zehmakan, Effective vaccination strategies in network-based SIR model, *Chaos Soliton. Fract.*, **175** (2023), 113952. https://doi.org/10.1016/j.chaos.2023.113952
6. F. Arif, Z. Majeed, J. U. Rahman, N. Iqbal, J. Kafle, Mathematical modeling and numerical simulation for the outbreak of COVID-19 involving loss of immunity and quarantined class, *Comput. Math. Method. M.*, **2022** (2022), 3816492. https://doi.org/10.1155/2022/3816492
7. M. Farman, E. Hincal, P. A. Naik, A. Hasan, A. Sambas, K. S. Nisar, Fractional-order modeling of panic-driven human behavior during COVID-19 pandemic using the Caputo derivative, *Part. Differ. Equ. Appl. Math.*, **6** (2024), 101047. https://doi.org/10.1016/j.padiff.2024.101047
8. D. Choudhary, M. N. Srinivas, B. S. N. Murthy, P. A. Naik, K. S. Nisar, A review of the effect of environmental factors on COVID-19 disease, *Innov. Emerg. Technol.*, **12** (2025), 2530005. https://doi.org/10.1142/S2737599425300053
9. F. Murphy, Covid-19: New variant spreading across Asia is found in UK, *BMJ*, **389** (2025), r1161. https://doi.org/10.1136/bmj.r1161
10. C. Guo, Y. Yu, J. Liu, F. Jian, S. Yang, W. Song, et al., Antigenic and virological characteristics of SARS-CoV-2 variant BA.3.2, XFG, and NB.1.8.1, *BioRxiv*, 2025. https://doi.org/10.1101/2025.04.30.651462
11. A. Din, Y. Li, Optimizing HIV/AIDS dynamics: Stochastic control strategies with education and treatment, *Eur. Phys. J. Plus*, **139** (2024), 1–19. https://doi.org/10.1140/epjp/s13360-024-05605-1
12. A. Din, Bifurcation analysis of a delayed stochastic HBV epidemic model: Cell-to-cell transmission, *Chaos Soliton. Fract.*, **181** (2024), 114714. https://doi.org/10.1016/j.chaos.2024.114714
13. S. S. Ullah, A. Hasan, Y. T. Shih, A novel hybrid fractional approach to nonlinear dynamics of HIV transmission among men who have sex with men in Taiwan, *AIMS Math.*, **10** (2025), 13204–13230. https://doi.org/10.3934/math.2025592
14. A. Ramponi, M. E. Tessitore, Optimal social and vaccination control in the SVIR epidemic model, *Mathematics*, **12** (2024), 933. https://doi.org/10.3390/math12070933
15. A. Venkatesh, M. Manivel, K. Arunkumar, M. P. Raj, S. D. Purohit, A fractional mathematical model for vaccinated humans with the impairment of Monkeypox transmission, *Eur. Phys. J.-Spec. Top.*, **2024** (2024), 1–21. https://doi.org/10.1140/epjs/s11734-024-01211-5
16. K. Li, J. Rui, W. Song, L. Luo, Y. Zhao, H. Qu, et al., Temporal shifts in 24 notifiable infectious diseases in China before and during the COVID-19 pandemic, *Nat. Commun.*, **15** (2024), 3891. https://doi.org/10.1038/s41467-024-48201-8
17. P. Wu, Z. Feng, Global dynamics of a space-age structured COVID-19 model coupling within-host infection and between-host transmission, *Commun. Nonlinear Sci.*, **131** (2024), 107801. https://doi.org/10.1016/j.cnsns.2023.107801

18. W. O. Kermack, A. G. McKendrick, A contribution to the mathematical theory of epidemics, *P. Roy. Soc. A*, **115** (1927), 700–721. https://doi.org/10.1098/rspa.1927.0118

19. I. U. Haq, N. Ullah, N. Ali, K. S. Nisar, A new mathematical model of COVID-19 with quarantine and vaccination, *Mathematics*, **11** (2023), 142. https://doi.org/10.3390/math11010142

20. O. Diekmann, J. A. P. Heesterbeek, J. A. J. Metz, On the definition and the computation of the basic reproduction ratio R_o in models for infectious diseases in heterogeneous populations, *J. Math. Biol.*, **28** (1990), 365–382. https://doi.org/10.1007/BF00178324

21. O. Diekmann, J. A. P. Heesterbeek, M. G. Roberts, The construction of next-generation matrices for compartmental epidemic models, *J. R. Soc. Interface*, **7** (2010), 873–885. https://doi.org/10.1098/rsif.2009.0386

22. J. P. LaSalle, Stability theory and invariance principles, *Dynam. Syst.*, **1** (1976), 211–222. https://doi.org/10.1016/B978-0-12-164901-2.50021-0

AIMS Press